Earth and Planetary Science Letters 501 (2018) 119–127

Contents lists available at ScienceDirect

Earth and Planetary Science Letters

www.elsevier.com/locate/epsl

Ambient seismic vibrations in steep bedrock permafrost used to infer variations of ice-fill in fractures

S. Weber [a,*], D. Fäh [b], J. Beutel [c], J. Faillettaz [a], S. Gruber [d], A. Vieli [a]

[a] Department of Geography, University of Zurich, Switzerland
[b] Swiss Seismological Service, ETH Zurich, Switzerland
[c] Computer Engineering and Networks Laboratory, ETH Zurich, Switzerland
[d] Carleton University, Ottawa, Canada

ARTICLE INFO

Article history:
Received 30 May 2018
Received in revised form 19 August 2018
Accepted 22 August 2018
Available online xxxx
Editor: M. Ishii

Keywords:
bedrock permafrost
ambient seismic vibration
fracture displacement

ABSTRACT

The behavior of ice in frozen rock masses is an important control on rock slope stability but the knowledge of the formation, extent and evolution of ice-filled fractures in steep bedrock permafrost is limited. Therefore, this study aims at characterizing the site specific ambient seismic vibration recorded at the Matterhorn Hörnligrat fieldsite over the course of more than three years. The observed normal mode resonance frequencies vary seasonally with four distinct phases: persistent decrease during summer (phase I), rapid increase during freezing (phase II), trough-shaped pattern in winter (phase III) and a sharp peak with a rapid decay during the melting/thawing season (phase IV). The relation between resonance frequency and rock temperature exhibits an annually repeated pattern with hysteretic behavior. The link between resonance frequency, fracture width and rock temperature indicates that irreversible fracture displacement is dominant in summer periods with low resonance frequency. These findings suggest that the temporal variations in resonance frequencies are linked to the formation and melt of ice-fill in bedrock fractures.

1. Introduction

Destabilization of steep bedrock permafrost is a natural hazard that potentially endangers populated mountain areas (Haeberli et al., 2010) as permafrost responds rapidly to climate change related warming (Deline et al., 2015), which leads to a change in the rock properties and in the processes controlling rock slope stability (Krautblatter et al., 2013). While the thawing of intact water-saturated rock results in a significant strength reduction (Mellor, 1973), the shear resistance of ice-filled discontinuities decreases with rising temperature and reaches a minimum just below 0 °C (Davies et al., 2001; Günzel, 2008). Rockfall events at several locations and with different volumes (from 10^3 to $>10^6$ m^3) have uncovered ice in the formerly buried detachment zone (e.g. Hasler et al., 2012). The formation of ice within rock often causes damage ranging from near-surface (Hallet et al., 1991) to the depth of several meters (Murton et al., 2006) and therefore may play a role in the destabilization of rock slopes and in preconditioning of rockfall (Gruber and Haeberli, 2007; Matsuoka and Murton, 2008). At the same time, the hydraulic permeability is much lower in rock masses with frozen and ice-filled fissures than in unfrozen fissures. This effect often leads to high hydrostatic stress due to perched water (Pogrebiskiy and Chernyshev, 1977). Further, no hydrostatic stress can develop in fractures completely filled with ice, but can change rapidly when the frozen fractures thaw.

There is only limited knowledge of the formation, extent and evolution of ice-filled fractures in steep bedrock permafrost. Characteristic patterns in relative surface displacement data have often been associated to cryogenic processes (e.g. Draebing et al., 2017), but no or only limited evidence was provided. A few studies measured electrical resistivity tomography (ERT) in solid rock faces (Sass, 2005) as well as in solid permafrost rock walls (Krautblatter and Hauck, 2007) and thereby observed temporal and spatial variations of moisture movement during freeze-thaw cycles. Further geophysical methods were semi-successfully applied directly in fractures to monitor changes in ice-infill of fractures, for example compression stress measurements (Hasler et al., 2012) or water pressure in fractures (Draebing et al., 2017).

Passive monitoring of elastic waves (either the detection of seismic events and/or the recording of ambient seismic vibrations) provides subsurface information within a delimited perimeter and can complement surface displacement measurements. In non-permafrost areas this method has been widely applied (i) to characterize the seismic response of unstable rock slopes

* Corresponding author.
E-mail address: samuel.weber@geo.uzh.ch (S. Weber).

https://doi.org/10.1016/j.epsl.2018.08.042
0012-821X/

(Moore et al., 2011; Bottelin et al., 2013a; Kleinbrod et al., 2017a; Burjánek et al., 2018), (ii) to study fracturing processes and factors influencing rock slope destabilization (e.g. Helmstetter and Garambois, 2010), (iii) to identify precursory behavior prior to slope failure (e.g. Amitrano et al., 2005; Lévy et al., 2010) or (iv) to detect small size rockfalls (e.g. Lacroix and Helmstetter, 2011).

Recordings of ambient seismic noise, which consists of ground vibrations that are not induced by seismic events, provide information about site specific resonance frequencies (Del Gaudio et al., 2014). Resonance describes an amplification of ground motion at a specific frequency, but often occurs manifold with different frequencies. These resonance frequencies are related to material properties and provide information on internal structure and geometry (e.g. depth and volume) of an unstable rock slope (Burjánek et al., 2012; Gischig et al., 2015). The characterization of variations in these resonance frequencies has been recognized as an important approach to identify permanent changes associated with internal rock mass damage (Burjánek et al., 2018). For example, seasonal variations of resonance frequencies in an unstable rock column were linked to the temperature dependent bulk elastic properties and related closure of fracture rock bridges due to the thermally induced expansion of rock or the formation of ice (Bottelin et al., 2013b).

Applications of passive monitoring of acoustic emissions and micro-seismic events in bedrock permafrost have gained in popularity in the last decade (e.g. Amitrano et al., 2010; Weber et al., 2018) but still experience difficulties in analysis and interpretation (Weber et al., 2018). And so far, the seismic response of bedrock permafrost based on ambient seismic vibration analysis is largely unexplored.

In this study, we aim to analyze ambient seismic noise recorded in steep, fractured bedrock permafrost at the Matterhorn Hörnligrat fieldsite over the course of more than three years. We critically interpret this dataset in relation to variations in external environmental forcing and investigate the working hypothesis that ambient seismic noise can provide evidence for the formation and melt out of ice-fill in fractures.

In the first part of this manuscript, we describe the measurement setup in the field, analysis methods and results derived from the recorded time series of ambient seismic noise, fracture displacement and temperature in the active layer of steep and fractured bedrock permafrost (Sections 2–4). We then elaborate on typical patterns observed, interpret relations found within these data and discuss the working hypothesis formulated above.

2. Matterhorn Hörnligrat fieldsite and instrumentation setup

The Matterhorn Hörnligrat fieldsite (see Fig. 1a) is located at an elevation of 3500 m a.s.l. on the North-East ridge of the Matterhorn in the Swiss Alps. This fieldsite is characterized by extensive structuring and the occurrence of ice-filled fractures (Hasler et al., 2012), a heterogeneous surface with debris-covered ledges and recurring patterns of snow cover (Weber et al., 2017). Geologically, this fieldsite is located above the Penninic Metasediments and Ophiolites (Combin Zone) and consists of gneiss and amphibolite of the Dent Blanche nappe (Bucher et al., 2004). There are many vertical rifts and the main fractures in the study area are oriented parallel to the ridge with a nearly vertical dip (Hasler et al., 2012). Local permafrost with an active layer of several meters is estimated on the south side while extensive permafrost with a thin active layer of few meters is observed on the north side (Weber et al., 2018). A detailed fieldsite description is given by Hasler et al. (2012) and Weber et al. (2017, 2018).

The instrumentation setup relevant for this study is shown in Fig. 1 and consists of (i) two three-component seismometers (Lennartz electronic low-noise seismometer LE-3Dlite MKIII with a 1 Hz to 100 Hz passband and Nanometrics Centaur digital recorder, a 24-bit high-resolution seismic data acquisition system paced by GPS with a sampling rate of 1000 sps), (ii) one crackmeter (perpendicular to fracture, recorded at 2 min intervals with an accuracy of ±0.01 mm), (iii) one thermistor sensor rod measuring rock temperature at different depths (5, 10, 20, 30, 50 and 100 cm at 2 min intervals with an accuracy of ±0.2 °C) and (iv) a weather station (Vaisala WXT520 providing wind and air temperature data recorded at 2 min intervals). For precipitation, the MeteoSwiss SwissMetNet surface weather station Zermatt at an elevation of 1638 m a.s.l. was used. The recording at the Matterhorn Hörnligrat fieldsite started in June 2015. There are a few short gaps (few days) in all data and considerable gaps (several months) in the weather station data because of a system failure. Note, we do not aim to detect and localize micro-seismic events and thus two seismometer stations are sufficient.

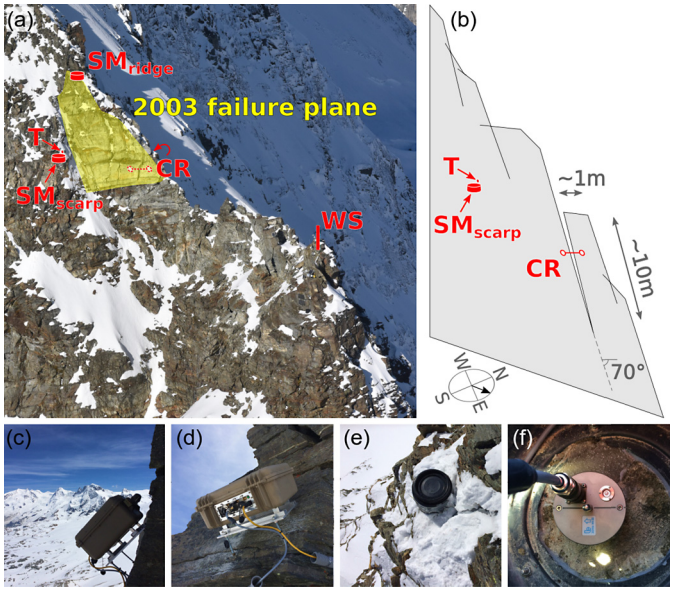

Fig. 1. Detailed view on the Hörnligrat fieldsite on the North-East ridge of the Matterhorn in the Swiss Alps at an elevation of 3500 m a.s.l. with an average slope >60°. The seismometers SM_{scarp} and SM_{ridge} are protected against mechanical damage with a bucket whereat the bucket of SM_{ridge} was filled with sand from 27 July 2015 until 18 July 2017 to reduce the signal noise (following the guidelines of Bard and SESAME Team, 2006). The temperature sensor rod *T* is mounted into a 1 m borehole next to the seismometer SM_{scarp}. The crackmeter CR is installed on the north-facing back site of the ridge (CR refers to the crackmeter *mh*03 in Weber et al., 2017) while the weather station WS is located on the ridge (WS refers to the location *mh*25 in Weber et al., 2017). (a) shows an aerial picture and (b) shows a schematic sketch while (c)–(f) show the seismometer setup. While the digitizer is deployed in a waterproof Peli case (c–d), the seismometer itself is mounted to the rock surface and protected with a bucket (e–f). (This figure is available in color in the web version of this article.)

3. Methods

3.1. Ambient seismic noise analysis

The Fourier amplitude spectrum was estimated for non-overlapping windows (10 min) of the recorded ambient seismic vibrations time series for each component of both seismometers. For this, first, the analysis toolbox provided by Prieto et al. (2009) was used to estimate the multitaper spectrum $\hat{S}(f)$:

$$\hat{S}(f) = \frac{\sum_{k=0}^{K-1} d_k^2 |Y_k(f)|^2}{\sum_{k=0}^{K-1} d_k^2}, \quad (1)$$

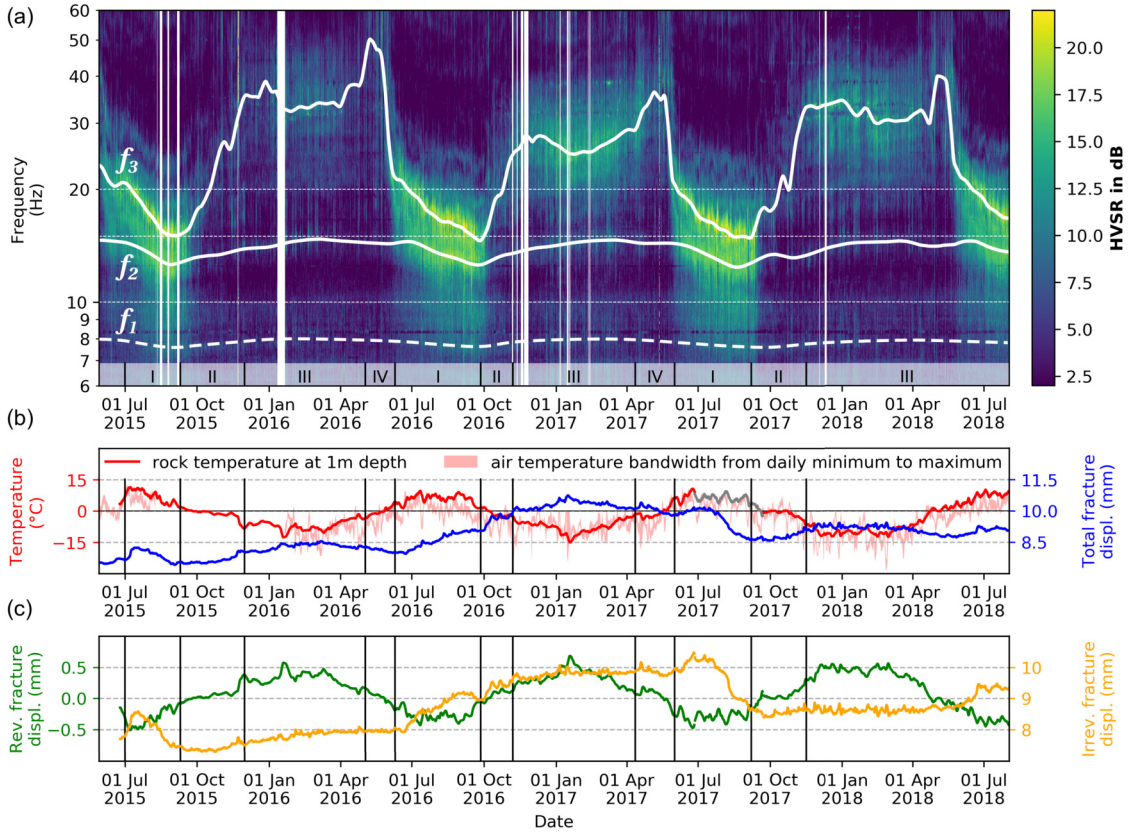

Fig. 2. (a) HVSR for SM_{scarp}: geometric mean of six 100 s windowed Fourier amplitude spectra after Prieto et al. (2009, Python wrapper implemented by Krischer, 2016), where the geometric mean of the horizontal components (North and East) was divided by the vertical component (Z). White lines highlight three dominant resonance frequencies where f_2 and f_3 were determined automatically with an Gaussian filter while f_1 was picked manually. (b) shows the measured rock temperature at 1 m depth in red and the measured fracture displacement in blue. (c) Quantification of reversible (green) and irreversible (orange) fracture displacement according to Weber et al. (2017), whereas positive values refer to opening and negative ones to closing. The irreversible fracture displacement, which is the residual displacement after removing the thermo-elastic component, exhibits a closing pattern in summer 2017. This changing pattern has been observed for the first time since summer 2008 indicating a change in the kinematics behavior of this fracture. A gap in the temperature time-series was filled, applying quantile mapping using the best regressors approach (Staub et al., 2017) and indicated with gray (b). (For interpretation of the colors in the figure(s), the reader is referred to the web version of this article.)

where $Y_k(f)$ is the k eigencomponent and d_k is the adaptive weight proposed by Thomson (1982). This method prevents spectral leakage, which describes frequency mixing with neighboring bins as a consequence of finite Fourier transformation and, therefore, does not require additional smoothing. This method was applied to subsets of 100 s length with 4 tapers and a time-bandwidth product of 2.5 using the Python wrapper by Krischer (2016). Then, these subsets were aggregated as 10 min averages (geometrical mean). These spectra now allow time- and frequency-dependent analysis of the ambient seismic vibration.

Horizontal-to-vertical spectral ratio (HVSR) of ambient seismic noise, also known as Nakamura method (Nakamura, 1989) is a reconnaissance technique to reveal site resonance in soft sediments conditions by detecting peaks in the spectral ratio whereby the nature of the noise field does not alter the results (for an overview, see Del Gaudio et al., 2014). While HVSR mainly reflects the S-wave resonance, several studies showed a relation between HVSR and the ellipticity of fundamental mode Rayleigh waves (e.g. Bard, 1998). There is some correlation between HVSR and the site amplification at the fundamental frequency of resonance. Nevertheless, many studies have shown its ability to reveal reliable information on site response in flat and horizontally layered sites (e.g. Bard, 1998) but also in more complex rock slopes (e.g. Jongmans et al., 2009). A contrast in seismic impedance at the boundary between fractured and intact rock mass results in the development of standing waves (normal mode vibration) as damaged rock with air-filled voids represents a volume with reduced elastic moduli (Burjánek et al., 2012).

Site-to-reference spectral ratio (SRSR) represents the relative, frequency-dependent amplification of a station (site) with respect to another station (Spudich et al., 1996) and has been primarily applied to earthquake recordings where the site-to-source distance is usually well constrained (Burjánek et al., 2014). Although the sources of noise are usually not known, SRSR can also be applied to ambient vibration data assuming the sources of noise are far away from the stations compared to the distance between the stations (Burjánek et al., 2012). The SRSR technique thereby strives to eliminate source and path specific effects and can be used to identify the fundamental frequency of a whole rock slope or blocks (Kleinbrod et al., 2017b).

3.2. Fracture displacement analysis

Surface displacement measurements in bedrock permafrost reveal a clear reversible (elastic) component related to thermal expansion (e.g. Hasler et al., 2012). Removing this reversible component from the observed displacement enables to quantify the residual (irreversible, plastic) component due to other processes. Weber et al. (2017) proposed an approach based on a linear regression model for separating these components and thereby allows a systematic analysis of fracture kinematics.

4. Results and interpretation

Fig. 2 shows a two-year time series of (a) the HVSR, (b) rock as well as air temperature and fracture displacement recordings and

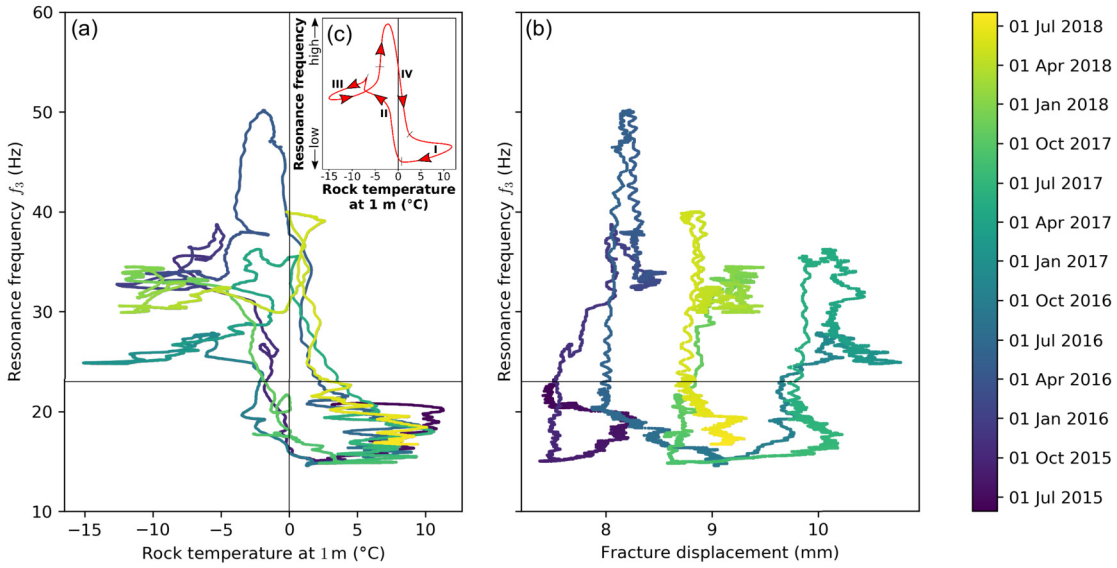

Fig. 3. For station SM_{scarp}: Relation between resonance frequency f_3 and (a) rock temperature and (b) fracture displacement over the course of more than three years respectively, where color indicates the time. (c) shows a schematic generalization of the rock temperature dependency of resonance frequency. Relation between resonance frequency and fracture displacement after separating reversible from irreversible component is shown in Fig. A.8. The same relation for resonance frequency f_2 are shown in Figs. A.9 and A.10. (For interpretation of the colors in the figure(s), the reader is referred to the web version of this article.)

(c) the separated fracture displacement components (reversible and irreversible) according to Weber et al. (2017). The coincident occurrence of a set of resonance frequencies can be the result of several unstable rock masses with different size overlying a bigger geological structure (e.g. Moore et al., 2011; Gischig et al., 2015). The three identified resonance frequencies (f_1, f_2 and f_3) with seasonal fluctuation are indicated in white (Fig. 2a). The intensity of the HVSR and the resonance frequencies vary seasonally with winter periods exhibiting increased resonance frequencies but smaller intensities in the HVSR (see Fig. 2a and Fig. 4a–b). These smaller intensities in the HVSR indicate reduced resonance. The seasonal pattern in resonance frequencies is reoccurring every year with all resonance frequencies (f_1, f_2, f_3) reaching their minima in summer and their maxima in winter. The seasonal fluctuation of the resonance frequency f_3 can visually be split into four different phases that correspond to distinct periods with specific thermal conditions (indicated with roman numbers in Fig. 2a): persistent decrease during summer (phase I), rapid increase during freezing (phase II), trough-shaped pattern in winter (phase III) and a sharp peak with a rapid decay during the melting/thawing season (phase IV). A fourth but lower resonance frequency (f_0) in the range 4–6 Hz is suggested by the HVSR-spectra in Fig. 4a and b. The small but wide amplitude, which might be strongly influenced by wind, impede an accurate tracking of this f_0 frequency peak and therefore is not analyzed in this study.

Fig. 3 visualizes the evolution of the resonance frequency f_3 in relation to (a) the rock temperature measured at 1 m depth and (b) the surface displacement recorded at a fracture a few meters away. The resonance frequency f_3 shows a repeated seasonal pattern with a hysteresis character, which is sketched out in Fig. 3c. The elliptic shaped orbit in this resonance-temperature diagram suggests a phase lag and dampening due to the subsurface conductive heat-transfer regime (Beltrami, 1996). Assuming the crackmeter is mounted on the rock mass producing the observed resonance frequency, the irreversible fracture displacement occurs during periods with low resonance frequency and with high temperature, which is supported by Fig. A.8.

5. Discussion

5.1. Influence of instrumentation and anthropogenic activity

It is unlikely that the instrumentation setup (i.e. protection bucket, cable routing or mounting, see Fig. 1c–d) causes the highest observed resonance frequencies f_3 due to the three following observations: (1) The protection bucket of plastic exhibits a low thermal capacity due to its small weight and, therefore, reacts quickly to changes in air temperature. No evident shift in the HVSR peak can be observed in summer during bad weather periods with strong cooling (see Fig. 2). Fig. 4c shows the HVSR spectra for time windows before, during and after a bad weather period with temperatures considerably below 0 °C (from 13 July to 15 July 2016) but no shift in HVSR is apparent. The mentioned phase between resonance frequency and rock temperature (see Fig. 3 and A.9) supports the independence between instrumentation setup and obtained resonance frequencies. (2) The protection bucket of the SM_{ridge} was filled with sand for almost two years (sand filling on 27 July 2015 and sand removal 18 July 2017 are indicated with red and black, vertical lines in Fig. 5). The sand infill considerably changes the weight and mechanical properties of the protection. Though if resonance frequency f_3 at SM_{scarp} was induced by the protection bucket, we would expect to recognize the sand fill intervention in the SRSR (see Fig. 5b). Further, no strong change in the HVSR pattern for the SM_{ridge} with this intervention is apparent (see Fig. 5a). However, if we only considered SRSR, resonance frequency f_2 would be favored as the resonance of the overlying rock mass. (3) Environmental factors, such as precipitation (rain, snow or hail), wind and snow cover can affect the recorded data by influencing the instrumentation setup heavy through for example vibrations of the bucket or cables. All these factors reflect the weather, which can change very quickly but also be persistent. If one of these factors induced a dominant change in the observed resonance frequencies, there would be many changes all year long as there are good and bad weather periods in any season. Further, there are periods with snow in summer but also some without in winter (see Fig. 4 in Weber et al., 2017).

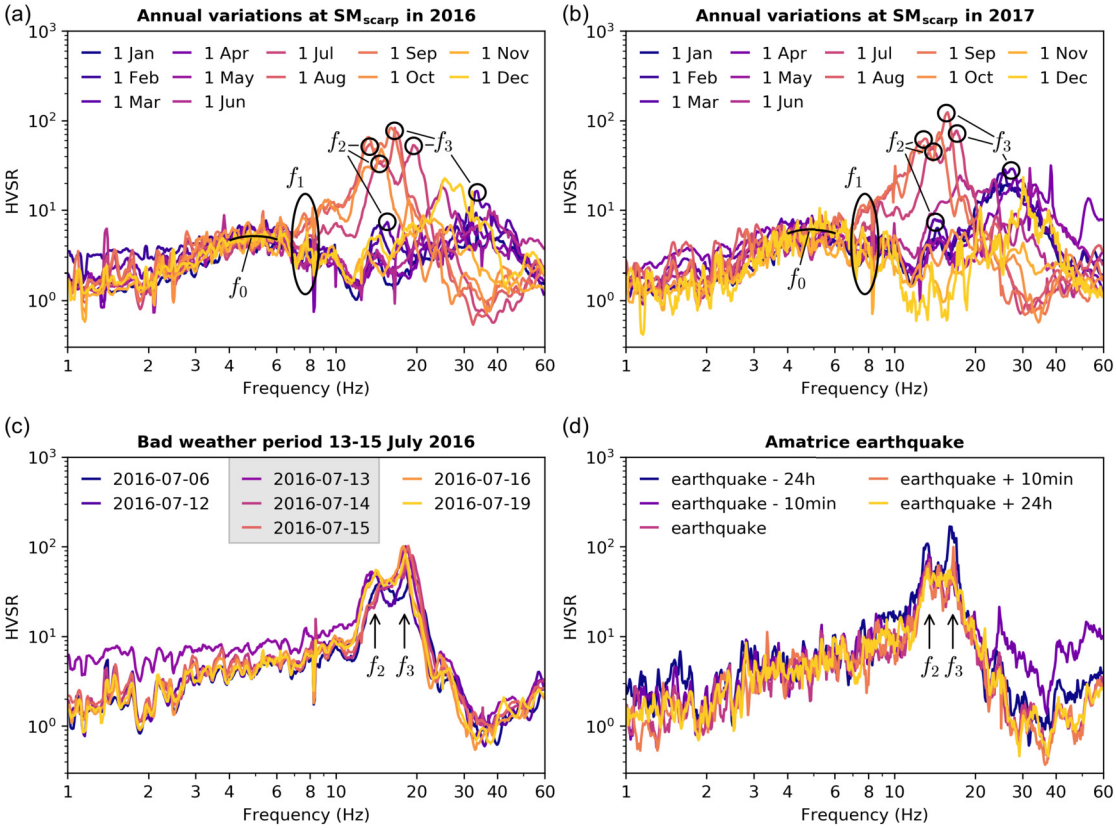

Fig. 4. Daily average of the HVSR of station SM$_{scarp}$ for the first day of each month over the entire year 2016 (a) and 2017 (b). Wile the black ellipsoid indicates the reference frequency f_1, the black circles refer to the resonance frequencies f_2 and f_3 for March, July and August. (c) Daily average of the HVSR of station SM$_{scarp}$ before/during/after bad weather period (13–15 July 2016) with strong cooling in summer. (d) HVSR for 10 min time windows of station SM$_{scarp}$ response to Amatrice earthquake (M6.2 on 24 August 2016, 03:36 in UTC+2:00). (For interpretation of the colors in the figure(s), the reader is referred to the web version of this article.)

Weber et al. (2018) showed seismic noise from anthropogenic activity (i.e. mountaineering or helicopter flights) to confound the analysis of seismic events with the exception of night hours. However, the present analysis does not show an apparent difference between consecutive and independent periods with and without mountaineering activity (verified with the time-lapse camera, see Weber et al., 2018).

Fig. 4d shows the HVSR spectra for the period coincident with the Amatrice earthquake and for two periods before and after the earthquake respectively. The similar pattern in the HVSR spectra indicates that earthquakes stimulate the same resonance frequency as ambient seismic vibrations do.

5.2. Driving processes and environmental forcing

The occurrence of several resonance frequencies suggests that this rock slope is composed of different rock volumes ranging from small blocks to a bigger geological structure (Moore et al., 2011) or that this rock slope exhibits heterogeneous characteristics with diverse material properties or local geological features (Burjánek et al., 2012; Gischig et al., 2015). Resonance frequency f_2 could potentially be a multiple of f_1, but the tracking of f_1 is subject to considerable uncertainty.

A variety of processes occur in mountain permafrost or its active layer, but two according properties are distinct for steep bedrock sites. On the one hand, high thermal gradients in the ground result from intense radiation in snow-free areas with high daily fluctuations in air temperature and the exponential damping of the surface temperature variations with depth (Williams and Smith, 1991). On the other hand, seasonal periods with longer sustained freezing or thawing and periods with repeated freeze-thaw cycles occur. Two distinct processes of ice formation, namely in situ freezing with volumetric expansion and ice segregation with migration of water to the freezing front can occur depending on the freezing rate and duration, the water availability and the properties of the rock (Matsuoka and Murton, 2008). While the volumetric expansion of freezing water is an important physical process, studies in the early twentieth century (e.g. Taber, 1930) already demonstrated that frost damage can not solely be explained with volume expansion. However, ice segregation in crystalline rock acts very slowly and is unlikely due to the low rock porosity, which leads on to a low water availability and limits the permeability (Murton et al., 2006).

While the exact process is unclear, freezing appears to be also reflected in the suggested four-phase seasonal pattern of resonance frequency f_3 in Fig. 2. Phases II (increase with freezing period) and IV (sharp peak with a strong decay in the melting/thawing season) could be explained by the formation and melt of ice. While an overall, seasonal cooling occurs in phase II (freezing) and most available water (trapped in pores or perched in fractures) freezes, phase IV (spring) coincides with the melt of the snow cover. This melt water percolates into fractures and there becomes available for refreezing in cold rock with a period of a few hours to a few days. The subsequent strong decay in resonance frequency f_3, which is indicated by positive rock temperature values, coincides with the process of melting or thawing. The summer period (phase I) is characterized by a persistent decrease, which stops abruptly with the onset of negative rock temperatures and thereby leads on to the phase II (freezing).

Bottelin et al. (2013a) presented similar findings describing seasonal variations in resonance frequencies, but with almost constant values in summer and winter. By contrast, our results exhibit spe-

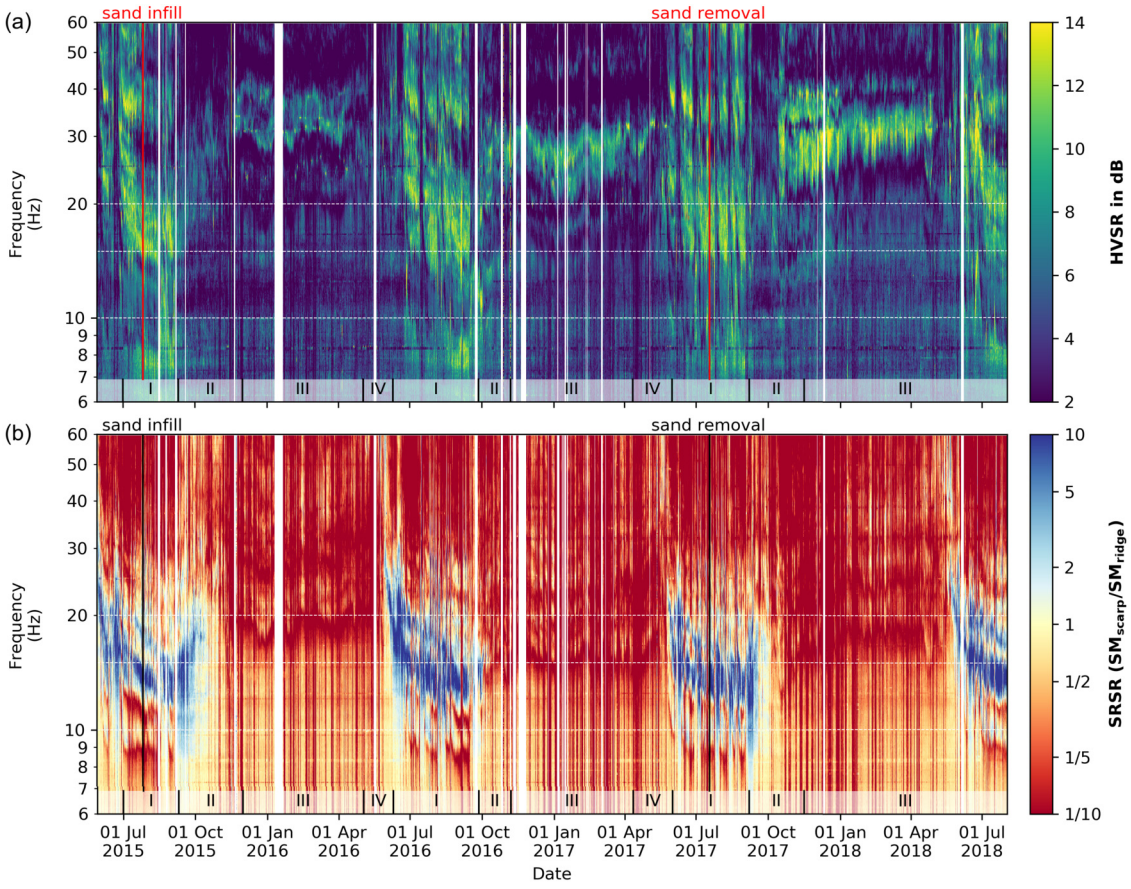

Fig. 5. (a) HVSR for SM_{ridge}: geometric mean of six 100 s windowed Fourier amplitude spectra after Prieto et al. (2009, Python wrapper implemented by Krischer, 2016), where H refers to the geometric mean of the horizontal components (North and East) and V to the vertical component (Z). (b) shows the site-to-reference spectral ratio SM_{scarp}/SM_{ridge}. Red and black solid lines indicate when sand was infilled (left) and removed (right) at SM_{ridge}, but no apparent change is visible. The roman numbers refer to the four phases in Fig. 2. (For interpretation of the colors in the figure(s), the reader is referred to the web version of this article.)

cific patterns in summer (phase I in Fig. 2) and winter (phase III in Fig. 2). The reducing degression in resonance frequency f_3 during summer could be explained by a decreasing melt rate with greater depth due to the phase lag and damping of temperature. The characteristic parabolic pattern in phase III (winter) occurs periodically every winter, but there is no evident explanation so far. The decrease in the resonance frequency during the first part of the phase could be related to the transformation of snow to firn/ice in the fractures. The subsequent increase could be caused by further fill up of the fracture with snow. In this case, we would expect a relation between the seasonally varying resonance frequencies in winter (phase III) and the accumulated amount of snow. However, precipitation data measured at the MeteoSwiss SwissMetNet surface weather station Zermatt features only a marginal higher cumulative precipitation for the hydrological year 2015/2016 coincident with a higher resonance frequency peak compared to the hydrological year 2016/2017 (see Fig. A.11). The fact that the snow input to fractures may be much more complex than flat-field accumulation, mainly due to wind, needs to be taken into account (Weber et al., 2017). Furthermore, Lévy et al. (2010) interpreted a significant drop in resonance frequency during freeze-thaw cycles as the result of rock bridge breakage.

Lévy et al. (2010) and Bottelin et al. (2013a) suggested that closure/opening of the hidden fracture rock bridges due to thermal expansion/contraction of rock reflects in an increase/decrease of the resonance frequencies, as closure of the hidden fracture causes a stiffening due to the contact between the rock volumes. However, the analysis of the fracture displacement data recorded at the Matterhorn Hörnligrat fieldsite exhibits a behavior with opposite sign (see Fig. 2b and c).

In addition to the formation of ice and frost damage in bedrock permafrost, the wave velocity in rock is temperature sensitive. Draebing and Krautblatter (2012) quantified the temperature dependent P-wave velocity with rock samples from the Matterhorn Hörnligrat fieldsite and highlighted a significant change when rock temperatures drop below 0 °C. Based on these laboratory experiment data (Fig. A.12a), we investigated the influence of temperature dependent P-wave velocity on the resonance frequency assuming a homogeneous temperature field. Note that a temperature dependency for the shear wave velocity is also expected, which has not been investigated to our knowledge. Ignoring the shear waves, we find that only a small portion of the resonance frequency fluctuation can be explained by the temperature dependent P-wave velocity (Fig. A.12). Therefore, we propose an alternative approach that is based on length variations of a cantilever beam substituting a rock mass.

5.3. Variation of ice-fill in bedrock fractures

Our results indicate a link between the resonance frequency f_3 and transition of temperature, though this relation is non-linear. The scenario of a rock mass adjoining a fracture, which is sketched out in Fig. 1b, raises the question if seasonal variations in resonance frequency are also related to changes of fracture depth or the level of ice-infill. A strongly simplified approach to address this question is to describe the temporally varying resonance frequency with changing length of a cantilever beam (Fig. 6a). The theoretical

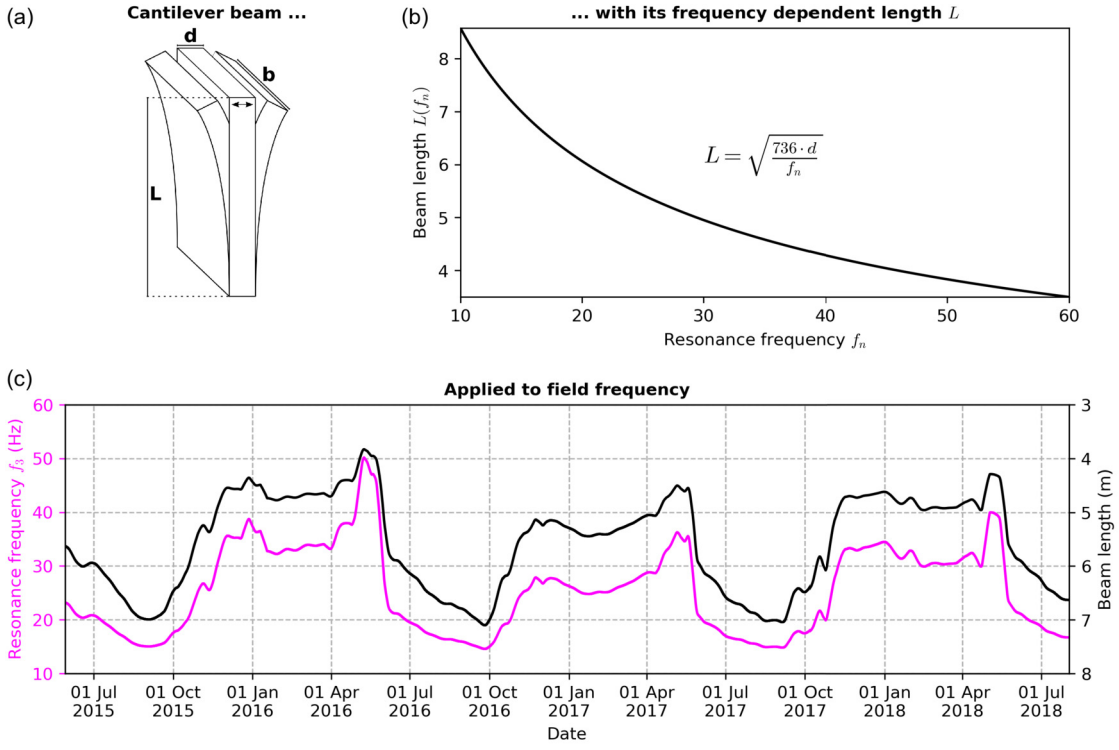

Fig. 6. Attempt to describe the temporally varying resonance frequency with a changing length of cantilever beam. (a) Sketch of a cantilever beam with (b) its theoretical beam length dependent resonance frequency based on Equation (2) (Landau and Lifshitz, 1986; Van Eysden and Sader, 2006). (c) Beam length derived from the measured resonance frequency f_3. (For interpretation of the colors in the figure(s), the reader is referred to the web version of this article.)

resonance frequency f_n dependent length L of a rectangular beam is:

$$L = \left(\frac{\alpha_n^2}{f_n \times 2\pi} \times \left(\frac{E \times I}{m} \right)^{0.5} \right)^{0.5}, \tag{2}$$

where α is a mode specific constant of the mode order n (nth positive root of $1 + \cos\alpha_n \cosh\alpha_n = 0$), E is Young's modulus, I is the moment of inertia of the beam cross section, and m is the mass per unit length of the beam (Landau and Lifshitz, 1986; Van Eysden and Sader, 2006). For a rectangular beam with edge lengths b and d ($b > d$), the ratio between the moment of inertia and the mass per unit length is:

$$\frac{I}{m} = \frac{\frac{1}{12} \times b \times d^3}{\rho \times b \times d} = \frac{d^2}{12 \times \rho}, \tag{3}$$

and, therefore, the frequency dependent length L of a beam results in:

$$L = \left(\frac{\alpha_n^2}{f_n \times 2\pi} \times \left(\frac{E \times d^2}{12 \times \rho} \right)^{0.5} \right)^{0.5}. \tag{4}$$

On the basis of a rock beam with a width of $d = 1$ m (visualized in Fig. 6b), a density of $\rho = 2700$ kg m^{-3} and the Young's modulus $E = 56 \cdot 10^9$ N m^{-2}, Equation (4) was applied to the resonance frequency time series (Fig. 6c) for the first natural frequency ($\alpha = 1.875$). Assuming the varying beam length represents the fracture depth from the surface down to the level of ice-infill, the seasonal pattern of the beam length corresponds to the expected evolution of ice formation in fractures. This approach has potential as a novel and simple means for stability assessment: A significant dip of the resonance frequency below its multi-annual minimum indicates a change in length or geometry of the resonating rock mass and the adjoining fractures. A drop below the annual minimum would be linked to severe fracture propagation potentially leading to rock slope destabilization presuming there are no developing fractures without a resonant response. However, in our case, the pattern of the resonance frequency is periodic over the years and thus is interpreted as not pointing to significant irreversible changes in fracture. The irreversible fracture displacement of a few millimeters recorded at the crackmeter (see Fig. 2) does not directly provide information of fracture depth as the rock mass is strongly fractured. Further, changes in resonance frequency due to fracture propagation might be negligible compared to variations in resonance frequency due to seasonal ice-infill. Further, the yearly minimum of resonance frequency f_3 (Fig. 2) is very stable (± 1 Hz) over the three-year time series indicating a negligible change in fracture depth due to fracture propagation.

Multiple evidence of ice-filled fractures exists at the Matterhorn Hörnligrat fieldsite: (i) A rockfall of approximately 1500 m^3 uncovered ice in the failure plane in summer 2003 (Hasler et al., 2012) and (ii) observations of ice in fractures during field visits in winter. We therefore propose the following scenario sketched out in Fig. 7: While the very bottom of the fracture is in permafrost where ice contained in fractures remains frozen, the main ice-fill changes are likely to occur in the active layer. The refreezing of percolating melt water from the surface snow (phase IV, melt onset) first causes an increase of ice-fill. Later on with continuing thawing, the ice melts. The melt water can easily escape through oblique fractures. Below these oblique fractures much slower melting with related lowering of the ice-infill (phase I, summer) is expected as melt water drains off without supplying energy to the remaining ice. Further, it is conceivable that a fracture is filled only partly and not completely starting from the bottom up. This would potentially lead to a step change in resonance frequency during freezing (phase II) and melt onset (phase IV). Gischig et al. (2011) concluded that the formation of ice in the freezing period causes deformation at depth. In permafrost bedrock, such seasonal

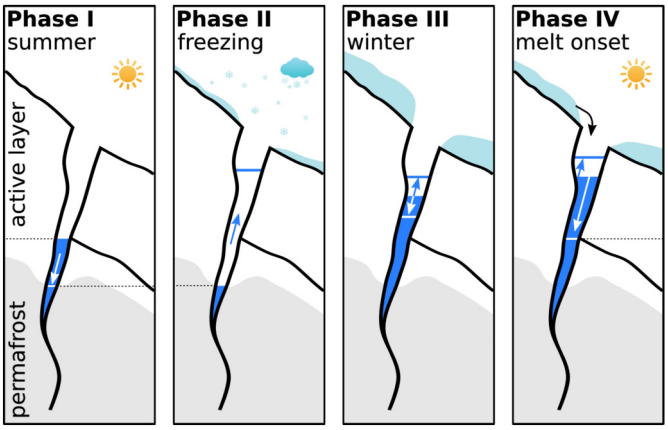

Fig. 7. Conceptual variation of ice-fill in a bedrock permafrost fracture. A lateral fracture in the active layer enables the run off of water during thawing periods. (This figure is available in color in the web version of this article.)

deformation could lead to water infiltration and thus promote the formation of additional ice at depth with enhanced irreversible deformation. In our study, no irreversible displacement was observed during freezing in winter (phase III) but during thawing in summer (phase I) without refreezing of percolating water. This observation is supported by up to a decade of fracture displacement measurements (Weber et al., 2017).

The filling of fractures has not necessarily to be solid ice, but could also consist of loose, fine material that is present at this field site. Such filling provides the capability to hold back water due to capillarity effects. Assuming water saturated material with a porosity of 40% freezes, a volumetric expansion of approximately 3–4% and stiffening of the fracture is expected. This effect potentially results in an increase of resonance frequency during freezing (see phase II in Fig. 2). In the preceding phase I (summer), slow settlement/subsidence of the filling material leads to a decrease in resonance frequency. However, rapid changes during freezing (phase II) and melt onset (phase IV) with such a delayed and slowed subsidence would be surprising. Note that fully saturated material is rather unlikely at the Matterhorn Hörnligrat fieldsite. Further, the quantification and determination of the fracture infill and properties has not been feasible so far.

Kleinbrod et al. (2017a) suggested in a non-permafrost study that the occurrence of resonance in a broad frequency band is an indication of stronger fracturing of the rock mass. We observed resonance in a broader frequency band during summer (phase I in Fig. 2 and June–August in Fig. 4) and in a rather narrow frequency band during the remaining time. This finding is consistent with a periodic, seasonal bonding of smaller fractures with ice. Hence, monitoring ambient seismic vibrations might serve as a tool to confine time periods of thawing-related rockfall events.

6. Conclusions

We have presented nearly three years of ambient seismic vibrations recorded in steep, fractured bedrock permafrost on Matterhorn. This data set was used to characterize the seismic response and monitor changes associated with environmental factors or internal processes. The dominant resonance frequencies vary seasonally with winter periods exhibiting increased resonance frequencies. These periodic variations in the resonance frequencies suggest a strong and robust relation with temperature changes or temperature related processes. Extensive quality control supports the conclusion that the instrumentation setup itself did not influence the results obtained. We attempted to describe a rock mass characterized by adjoining fractures with a cantilever beam analogue. The observed variations in resonance frequency thereby would reflect changes in beam length. As the relation between resonance frequency and environmental forcing is robust but non-linear, we suggest that variations of ice-infill in fractures change the geometry of the resonating rock mass. This link is supported by the occurring environmental conditions and the response time needed for the formation or melt out of ice. As we revealed the site resonance from ambient seismic noise recording, we put forward the working hypothesis that the analysis of ambient seismic noise may provide evidence for the formation and melt out of ice-fill in fractures. Accordingly, the resonance in a narrow frequency band during freezing periods indicates a periodic, seasonal bonding of smaller fractures with ice. Although we can not fully exclude other explanations, we presume that this approach contributes to progress in quantifying the relative change of fracture depth or the level of ice-infill respectively. However, in situ observation of ice-infill are needed to verify this link. Nevertheless, tracking the inter-annual evolution in resonance frequencies might be a powerful tool to investigate the evolution of the stability of frozen rock masses and to detect thawing-related rockfall events.

Author contributions

Samuel Weber in collaboration with all co-authors designed the field experiment. Samuel Weber prepared the data, performed all the data analysis and made the figures in Python 3 with input and advice from Donat Fäh as well as the other authors. Samuel Weber prepared the manuscript with critical revision and final approval from all co-authors.

Competing interests

There is no conflict of interest.

Acknowledgements

The work presented in this paper is part of the project X-Sense 2 and was financed by http://www.nano-tera.ch (ref. no. 530659). The data supporting the conclusions are available on request from the authors. We are grateful to Lucas Girard, for laying the cornerstone of this project by writing major elements of the project proposal. We are grateful to Martin Lüthi, Ulrike Kleinbrod, Matthias Meyer and Lukas Preiswerk for constructive comments and interesting discussion. We acknowledge the PermaSense team, especially Tonio Gsell, who provided valuable support with the development of measurement devices and with data management. We thank Andreas Hasler for support with the experiment design and installation.

Appendix A. Supplementary material

Supplementary material related to this article can be found online at https://doi.org/10.1016/j.epsl.2018.08.042.

References

Amitrano, D., Arattano, M., Chiarle, M., Mortara, G., Occhiena, C., Pirulli, M., Scavia, C., 2010. Microseismic activity analysis for the study of the rupture mechanisms in unstable rock masses. Nat. Hazards Earth Syst. Sci. 10 (4), 831–841.

Amitrano, D., Grasso, J., Senfaute, G., 2005. Seismic precursory patterns before a cliff collapse and critical point phenomena. Geophys. Res. Lett. 32 (8), L08314.

Bard, P., SESAME Team, 2006. Guidelines for the implementation of the H/V spectral ratio technique on ambient vibrations: measurements, processing and interpretations. SESAME European research project.

Bard, P.-Y., 1998. Microtremor measurements: a tool for site effect estimation. In: Proceeding of the Second International Symposium on the Effects of Surface Geology on Seismic Motion. Yokohama, Japan, pp. 1251–1279.

Beltrami, H., 1996. Active layer distortion of annual air/soil thermal orbits. Permafr. Periglac. Process. 7 (2), 101–110.
Bottelin, P., Jongmans, D., Baillet, L., Lebourg, T., Hantz, D., Lévy, C., Le Roux, O., Cadet, H., Lorier, L., Rouiller, J.-D., Turpin, J., Darras, L., 2013a. Spectral analysis of prone-to-fall rock compartments using ambient vibrations. J. Environ. Eng. Geophys. 18 (4), 205.
Bottelin, P., Lévy, C., Baillet, L., Jongmans, D., Guéguen, P., 2013b. Modal and thermal analysis of les arches unstable rock column (vercors massif, French Alps). Geophys. J. Int. 194 (2), 849–858.
Bucher, K., Dal Piaz, G.V., Oberhänsli, R., Gouffon, Y., Martinotti, G., Polino, R., 2004. Blatt 1347 Matterhorn. Geol. Atlas Schweiz 1:25 000, Erläut. 107. Bundesamt für Wasser und Geologie, Wabern.
Burjánek, J., Edwards, B., Fäh, D., 2014. Empirical evidence of local seismic effects at sites with pronounced topography: a systematic approach. Geophys. J. Int. 197 (1), 608–619.
Burjánek, J., Gischig, V., Moore, J.R., Fäh, D., 2018. Ambient vibration characterization and monitoring of a rock slope close to collapse. Geophys. J. Int. 212 (1), 297–310.
Burjánek, J., Moore, J.R., Yugsi Molina, F.X., Fäh, D., 2012. Instrumental evidence of normal mode rock slope vibration. Geophys. J. Int. 188 (2), 559–569.
Davies, M., Hamza, O., Harris, C., 2001. The effect of rise in mean annual temperature on the stability of rock slopes containing ice-filled discontinuities. Permafr. Periglac. Process. 12 (1), 137–144.
Del Gaudio, V., Muscillo, S., Wasowski, J., 2014. What we can learn about slope response to earthquakes from ambient noise analysis: an overview. Eng. Geol. 182 (Part B), 182–200.
Deline, P., Gruber, S., Delaloye, R., Fischer, L., Geertsema, M., Giardino, M., Hasler, A., Kirkbride, M., Krautblatter, M., Magnin, F., McColl, S., Ravanel, L., Schoeneich, P., 2015. Ice loss and slope stability in high-mountain regions. In: Shroder, J.F., Haeberli, W., Whiteman, C. (Eds.), Snow and Ice-Related Hazards, Risks and Disasters. Academic Press, Boston, pp. 521–561, Chapter 15.
Draebing, D., Krautblatter, M., 2012. P-wave velocity changes in freezing hard low-porosity rocks: a laboratory-based time-average model. Cryosphere 6 (5), 1163–1174.
Draebing, D., Krautblatter, M., Hoffmann, T., 2017. Thermo-cryogenic controls of fracture kinematics in permafrost rockwalls. Geophys. Res. Lett. 44 (8), 3535–3544.
Gischig, S., Moore, J.R., Evans, K.F., Amann, F., Loew, S., 2011. Thermomechanical forcing of deep rock slope deformation: 2. The Randa rock slope instability. J. Geophys. Res., Earth Surf. 116 (F4).
Gischig, V.S., Eberhardt, E., Moore, J.R., Hungr, O., 2015. On the seismic response of deep-seated rock slope instabilities – insights from numerical modeling. Eng. Geol. 193, 1–18.
Gruber, S., Haeberli, W., 2007. Permafrost in steep bedrock slopes and its temperature-related destabilization following climate change. J. Geophys. Res. 112 (F2), F02S18.
Günzel, F., 2008. Shear strength of ice-filled rock joints. In: Hinkel, K.M. (Ed.), Proceedings of the 9th International Conference on Permafrost, vol. 1. Fairbanks, USA, pp. 581–586.
Haeberli, W., Noetzli, J., Arenson, L., Delaloye, R., Gärtner-Roer, I., Gruber, S., Isaksen, K., Kneisel, C., Krautblatter, M., Phillips, M., 2010. Mountain permafrost: development and challenges of a young research field. J. Glaciol. 56 (200), 1043–1058.
Hallet, B., Walder, J., Stubbs, C., 1991. Weathering by segregation ice growth in microcracks at sustained subzero temperatures: verification from an experimental study using acoustic emissions. Permafr. Periglac. Process. 2 (4), 283–300.
Hasler, A., Gruber, S., Beutel, J., 2012. Kinematics of steep bedrock permafrost. J. Geophys. Res. 117 (F1), F01016.
Helmstetter, A., Garambois, S., 2010. Seismic monitoring of Séchilienne rockslide (French Alps): analysis of seismic signals and their correlation with rainfalls. J. Geophys. Res., Earth Surf. 115 (F3), F03016.
Jongmans, D., Bièvre, G., Renalier, F., Schwartz, S., Beaurez, N., Orengo, Y., 2009. Geophysical investigation of a large landslide in glaciolacustrine clays in the Trièves area (French Alps). Eng. Geol. 109 (1), 45–56.
Kleinbrod, U., Burjánek, J., Fäh, D., 2017a. On the seismic response of instable rock slopes based on ambient vibration recordings. Earth Planets Space 69 (1), 126.
Kleinbrod, U., Burjánek, J., Hugentobler, M., Amann, F., Fäh, D., 2017b. A comparative study on seismic response of two unstable rock slopes within same tectonic setting but different activity level. Geophys. J. Int. 211 (3), 1428–1448.
Krautblatter, M., Funk, D., Günzel, F., 2013. Why permafrost rocks become unstable: a rock-ice-mechanical model in time and space. Earth Surf. Process. Landf. 38 (8), 876–887.
Krautblatter, M., Hauck, C., 2007. Electrical resistivity tomography monitoring of permafrost in solid rock walls. J. Geophys. Res., Earth Surf. 112 (F2), F02S20.
Krischer, L., 2016. mtspec Python wrappers 0.3.2.
Lacroix, P., Helmstetter, A., 2011. Location of seismic signals associated with microearthquakes and rockfalls on the Séchilienne landslide, French Alps. Bull. Seismol. Soc. Am. 101 (1), 341.
Landau, L.D., Lifshitz, E.M., 1986. Theory of Elasticity, 3rd edition. Course of Theoretical Physics, vol. 7, pp. 1–187.
Lévy, C., Baillet, L., Jongmans, D., Mourot, P., Hantz, D., 2010. Dynamic response of the Chamousset rock column (western Alps, France). J. Geophys. Res., Earth Surf. 115 (F4), F04043.
Matsuoka, N., Murton, J., 2008. Frost weathering: recent advances and future directions. Permafr. Periglac. Process. 19 (2), 195–210.
Mellor, M., 1973. Mechanical properties of rocks at low temperatures. In: 2nd International Conference on Permafrost, Yakutsk. International Permafrost Association, pp. 334–344.
Moore, J., Gischig, V., Burjánek, J., Loew, S., Fäh, D., 2011. Site effects in unstable rock slopes: dynamic behavior of the Randa instability (Switzerland). Bull. Seismol. Soc. Am. 101 (6), 3110–3116.
Murton, J., Peterson, R., Ozouf, J.-C., 2006. Bedrock fracture by ice segregation in cold regions. Science 314 (5802), 1127–1129.
Nakamura, Y., 1989. A method for dynamic characteristics estimation of subsurface using microtremor on the ground surface. Q. Rep. RTRI 30 (1), 25–33.
Pogrebiskiy, M., Chernyshev, S., 1977. Determination of the permeability of the frozen fissured rock massif in the vicinity of the Kolyma hydroelectric power station. Cold Regions Research and Engineering Laboratory – Draft Translation 634, 1–13.
Prieto, G.A., Parker, R.L., Vernon III, F.L., 2009. A Fortran 90 library for multitaper spectrum analysis. Comput. Geosci. 35 (8), 1701–1710.
Sass, O., 2005. Rock moisture measurements: techniques, results, and implications for weathering. Earth Surf. Process. Landf. 30 (3), 359–374.
Spudich, P., Hellweg, M., Lee, W.H.K., 1996. Directional topographic site response at tarzana observed in aftershocks of the 1994 Northridge, California, earthquake: implications for mainshock motions. Bull. Seismol. Soc. Am. 86 (1B), S193.
Staub, B., Hasler, A., Noetzli, J., Delaloye, R., 2017. Gap-filling algorithm for ground surface temperature data measured in permafrost and periglacial environments. Permafr. Periglac. Process. 28 (1), 275–285.
Taber, S., 1930. The mechanics of frost heaving. J. Geol. 38 (4), 303–317.
Thomson, D.J., 1982. Spectrum estimation and harmonic analysis. Proc. IEEE 70 (9), 1055–1096.
Van Eysden, C.A., Sader, J.E., 2006. Resonant frequencies of a rectangular cantilever beam immersed in a fluid. J. Appl. Phys. 100 (11), 114916.
Weber, S., Beutel, J., Faillettaz, J., Hasler, A., Krautblatter, M., Vieli, A., 2017. Quantifying irreversible movement in steep, fractured bedrock permafrost on Matterhorn (CH). Cryosphere 11 (1), 567–583.
Weber, S., Faillettaz, J., Meyer, M., Beutel, J., Vieli, A., 2018. Acoustic and microseismic characterization in steep bedrock permafrost on Matterhorn (CH). J. Geophys. Res., Earth Surf. 123 (6), 1363–1385.
Williams, P., Smith, M., 1991. The Frozen Earth: Fundamentals of Geocryology. Studies in Polar Research. Cambridge University Press.